Materials Chemistry and Physics 130 (2011) 708–713

Contents lists available at ScienceDirect

Materials Chemistry and Physics

journal homepage: www.elsevier.com/locate/matchemphys

Surface analysis of localized corrosion of austenitic 316L and duplex 2205 stainless steels in simulated body solutions

Marjetka Conradi[a,*], Peter M. Schön[b], Aleksandra Kocijan[a], M. Jenko[a], G. Julius Vancso[b]

[a] Institute of Metals and Technology, Lepi pot 11, 1000 Ljubljana, Slovenia
[b] Materials Science and Technology of Polymers and MESA+ Institute for Nanotechnology, University of Twente, Enschede 7500 AE, The Netherlands

ARTICLE INFO

Article history:
Received 16 February 2011
Received in revised form 5 July 2011
Accepted 15 July 2011

Keywords:
Metals
Electrochemical techniques
Atomic force microscopy (AFM)
Corrosion

ABSTRACT

We report on cyclic voltammetry and *in situ* electrochemical atomic force microscopy (EC-AFM) studies of localized corrosion of duplex 2205 stainless steel (DSS 2205) and austenitic stainless steel of the type AISI 316L in two model solutions, including artificial saliva (AS) and a simulated physiological solution known as – Hank's solution (PS). The AFM topography analysis illustrated the higher corrosion resistance of DSS 2205 steel for the chosen range of electrochemical potentials that were applied to the steel surface in both solutions. In contrast, pitting corrosion was observed at the surface of AISI 316L steel, with the pits becoming more evident, larger and deeper, when the sample was electrochemically treated in the PS. On both surfaces the growth of corrosion products formed during the oxidation process was observed. As a result, depending on the sample's metallurgical structure, different types of oxides covered the surface close to the breakdown potential. We distinguished between the square-like type of oxides on the surface of the DSS 2205, and the AISI 316L with its ellipse-like oxide deposits. The X-ray photoelectron spectroscopy (XPS) revealed the chemical composition of the deposition products, which consisted of two main elements, Fe and Cr. However, the oxides of the alloying elements Ni and Mo were negligible compared to the bulk.

1. Introduction

Austenitic stainless steel of the type AISI 316L is known as the most commonly used orthopaedic and orthodontic bracket material because of its favourable mechanical properties, such as high tensile strength, and relatively good corrosion resistance in various aqueous environments [1]. However, it is regularly challenged by the aggressive environment in the human body, as it is highly susceptible to localized corrosion in environments containing chloride [2]. Therefore, austenitic stainless steels are currently often replaced with duplex stainless steels. The combination of the two phases, delta-ferritic and austenite phases, in its metallurgical structure gives this material its unique mechanical properties. In addition to high strength, these steels also exhibit improved corrosion characteristics in chloride-rich media due to the high Cr content in combination with Mo and Ni [3]. Chromium adds to the overall resistance through a passivation process by forming a complex spinel-type passive film (Fe, Ni)O(Fe, Cr)$_2$O$_3$. Molybdenum, however, increases the stability of the passive film and, therefore, the ability of the stainless steel to resist the localized corrosion, including pitting and crevice corrosion, particularly in environments containing chloride ions [3–10].

The corrosion behaviour of stainless steels in simulated physiological conditions has been studied by various authors employing different techniques [11–13]. Kocijan et al. [11] studied the corrosion behaviour of AISI 316L under both open circuit potentials and potentiostatic conditions. The concentration of the dissolved corrosion products in the form of released ions was determined by differential pulse polarography and inductively coupled plasma atomic emission spectrometry. The composition of the solid corrosion products formed on the surface was analyzed by energy-dispersive X-ray spectroscopy (EDS) and their morphology was investigated with scanning electron microscopy (SEM). The addition of complexing agents to the physiological solution increased the dissolution of the investigated material. Burstein and Liu [12] reported on pitting corrosion with AISI 316L in the presence of bovine serum. The experiments involved measurements of the current transients generated on microelectrodes under potentiostatic control below the pitting potential. Shahryari et al. [13] demonstrated that the electrochemical cyclic potentiodynamic polarization (CPP) of a biomedical grade 316LVM stainless-steel surface is a very efficient passivation method that can be used to significantly improve the general corrosion resistance of the

* Corresponding author. Tel.: +386 1 4701 972; fax: +386 1 4701 939.
E-mail address: marjetka.conradi@imt.si (M. Conradi).

0254-0584/$ – see front matter © 2011 Elsevier B.V. All rights reserved.
doi:10.1016/j.matchemphys.2011.07.049

material and thus its biocompatibility. An increased thickness of the CPP-formed passive film and its enrichment with Cr(VI) and oxygen were determined to be the origin of the generally increased corrosion resistance of the material. A few authors studied the influence of chloride solutions on the corrosion properties of both AISI 316L and 2205 duplex stainless steel (DSS 2205) [8]. Electrochemical testing of the two steels in a 0.9% (w/w) chloride solution indicated that the DSS 2205 had a wider passivation range than the AISI 316L [8]. Torres et al. [14] investigated DSS 2205 in a chloride solution after various heat treatments. Using the potentiostatic polarization method, each heat-treated sample was corrosion tested in a 0.9% (w/w) NaCl solution at 37 °C to estimate its corrosion rate. The results showed that the simulated sensitisation had an adverse influence on the corrosion resistance, indicating that the corrosion rate increased with increasing sensitisation temperatures. Souto et al. [3] studied the passivation and the resistance to pitting corrosion of duplex stainless steel DIN 17006 (21%Cr-7%Ni-2%Mo-2%Mn-1%Cu) in neutral and alkaline buffered solutions, with and without chloride ions. They showed that the presence of NaCl enhanced the metal's electrodissolution through the passive layer due to the presence of Cr and Ni in the alloy.

There is, however, only a limited number of atomic force microscopy (AFM)-based corrosion studies performed *in situ* in model solutions under electrochemical potentiostatic control. In addition to other methods, AFM results provide an independent source for understanding the local corrosion phenomena and can also be used for the prediction of local corrosion sites. Veleva et al. [15] studied the growth of passive layers on AISI 316L in a solution that simulates concrete pore environments contaminated with chloride ions. Here, AFM topography imaging was employed to distinguish the pitting corrosion in saturated $Ca(OH)_2$ and cement extract, with and without the addition of NaCl. Antony et al. [7] showed the aggressiveness of sulphate-reducing bacteria in a marine environment, which plays an important role in the corrosion of duplex stainless steels. The initiation of the attack was evident from scanning electron microscopy (SEM) and AFM studies.

In this paper we examine the topographic and surface-roughness changes of AISI 316L and DSS 2205 when electrochemically treated in two model solutions, artificial saliva (AS) and a simulated physiological solution called Hank's solution (PS), with an increased chloride-ion concentration. The standard electrochemical technique of cyclic voltammetry was accompanied with the applied electrochemical atomic force microscopy (EC-AFM) for *in situ* localized corrosion studies. We focused on the pitting corrosion as well as the growth of the deposition products, whose chemical composition was additionally characterized with X-ray photoelectron spectroscopy (XPS).

2. Experimental

2.1. Materials

The materials under investigation were duplex 2205 stainless steel (22.7% Cr, 5.7% Ni, 2.57% Mo, 1.37% Mn, 0.38% Si, 0.032% P, 0.03% C, 0.001% S in mass fraction) and austenitic AISI 316L stainless steel (17% Cr, 10% Ni, 2.1% Mo, 1.4% Mn, 0.38% Si, 0.041% P, 0.021% C, <0.005% S in mass fraction). The concentrations of Cr, Ni, Mn and Mo in both investigated materials were determined using inductively coupled plasma atomic emission spectroscopy (ICP-AES, ICP-AES Perkin Elmer Optima 3100 RL instrument), while the concentration of Si was determined gravimetrically (Mettler H35AR balance). A spectrophotometric method using a bismuth phosphomolybdate complex was applied for the determination of phosphorus. The blue complex formed was extracted with methyl isobutyl ketone. The absorbance was measured at 625 nm (Opton PM 6 spectrophotometer). The concentration of carbon was determined by the oxidation of the sample in an induction furnace by heating in an oxygen atmosphere to form CO_2, which was then measured with an infrared detector (Eltra CS-800 instrument). The measuring principle was based on the infrared-radiation-absorbing properties of the gases. In the case of N determination, the sample was melted at high temperatures up to 3000 °C in an electrically heated graphite crucible in the furnace. Its concentration was determined with a thermal conductivity detector (Eltra ON-900 instrument).

The starting materials for electrochemical examination were cut into discs of 15 mm diameter and 1 mm thickness in order to fit into the AFM holder. The samples were prepared by a mechanical procedure, initially ground with SiC emery paper down to 1000 grit prior to the electrochemical studies, and then rinsed with distilled water.

2.2. Model solutions

The electrochemical experiments were carried out in two solutions (chemicals from Merck, Darmstadt, Germany), i.e., the artificial saliva, AS (0.4 g L^{-1} NaCl, 0.4 g L^{-1} KCl, 0.795 g L^{-1} $CaCl_2{\cdot}2H_2O$, 0.780 g L^{-1} $NaH_2PO_4{\cdot}9H_2O$, 0.005 g L^{-1} $Na_2S{\cdot}9H_2O$, 1 g L^{-1} Urea) and the simulated physiological Hank's solution, PS (8 g L^{-1} NaCl, 0.40 g L^{-1} KCl, 0.35 g L^{-1} $NaHCO_3$, 0.25 g L^{-1} $NaH_2PO_4{\cdot}2H_2O$, 0.06 g L^{-1} $Na_2HPO_4{\cdot}2H_2O$, 0.19 g L^{-1} $CaCl_2{\cdot}2H_2O$, 0.41 g L^{-1} $MgCl_2{\cdot}6H_2O$, 0.06 g L^{-1} $MgSO_4{\cdot}7H_2O$, 1 g L^{-1} glucose).

2.3. Cyclic voltammetry (CV)

In this experiment, the specimens were embedded in a Teflon PAR holder, immersed into the solution and employed as a working electrode. A high-purity graphite rod served as the counter electrode, while Ag/AgCl served as the reference electrode. The voltammograms were recorded using a EG&G PAR PC-controlled potentiostat/galvanostat Model 263 with M252 and Softcorr computer programs.

2.4. Atomic force microscopy

The morphology changes of the specimens' surfaces in the AS and PS solutions were studied with a combined electrochemistry atomic force microscope (EC-AFM) consisting of a NanoScope IV multimode instrument (Veeco-Bruker/Digital Instruments, Santa Barbara, California) and an electrochemical potentiostat (PGSTAT 10, AUTOLAB, the Netherlands). The multimode AFM was equipped with a 12 μm scanner (E scanner). Contact mode imaging in the liquid was performed in the respective electrolyte in a closed fluid cell with an O-ring seal (ca. 50-μL inner-cell volume) connected to external vessels via tubing for the liquid exchange (ca. 2-mL total volume incl. tubing and syringe vessel). To probe the surface, narrow-legged SiN cantilevers (DNP, Veecoprobes, Camarillo, California) with nominal spring constants of 0.5 N nm^{-1} were used. For the electrochemical measurements, the AFM liquid cell was equipped with a Ag wire as a pseudo reference and a Pt wire as a counter electrode, while the steel substrate was connected as a working electrode to the electrochemical potentiostat. The potentiostat was interfaced with a personal computer running under GPES for Windows, version 4.9 (ECO Chemie). The surface scanning was performed typically at a speed of 1–2 lines s^{-1}. The NanoScope software version 5.12r5 was used for the image processing and the roughness analysis.

Following the independent CV results, we first ran a test cyclic polarization scan on each sample directly in the EC-AFM setup to check the contacts of the chosen electrodes. Finally, each sample was exposed to different potentiostatic conditions for a certain period of time, ranging from a few seconds to a few minutes, depending on the corrosion resistance of the surface.

2.5. X-ray photoelectron spectroscopy (XPS)

The passive layers on the alloy surface were formed under potentiostatic conditions for 1 h at potentials of 0 V and 1.5 V vs. Ag/AgCl. These potentials were chosen with reference to the characteristic features of the cyclic voltammograms. After the electrochemical preparation, the specimens were rinsed with distilled water, dried and transferred to the analyser chamber within an hour. The XPS measurements were performed using a VG Scientific Microlab 310F instrument, non-monochromatized Mg K_α radiation (E = 1253.6 eV) and a hemispherical electron analyser operating at a pass energy of 20 eV. The spectra were collected using Avantage 3.41V data-analysis software, supplied by the manufacturer. After a background subtraction, in accordance with Shirley [16], and processing with the CasaXPS software developed by Fairley [17], the XPS signals were separated into the contributions from the different species.

3. Results and discussion

3.1. Cyclic voltammetry

The cyclic voltammograms of the 2205 DSS and AISI 316L samples recorded in AS and PS solutions made it possible to ascribe the current-density peaks to the corresponding electrochemical processes taking place on the surface of the investigated materials. The cyclic voltammograms for DSS 2205 and AISI 316L were recorded at a scan rate of 50 mV s^{-1}, in the potential range from

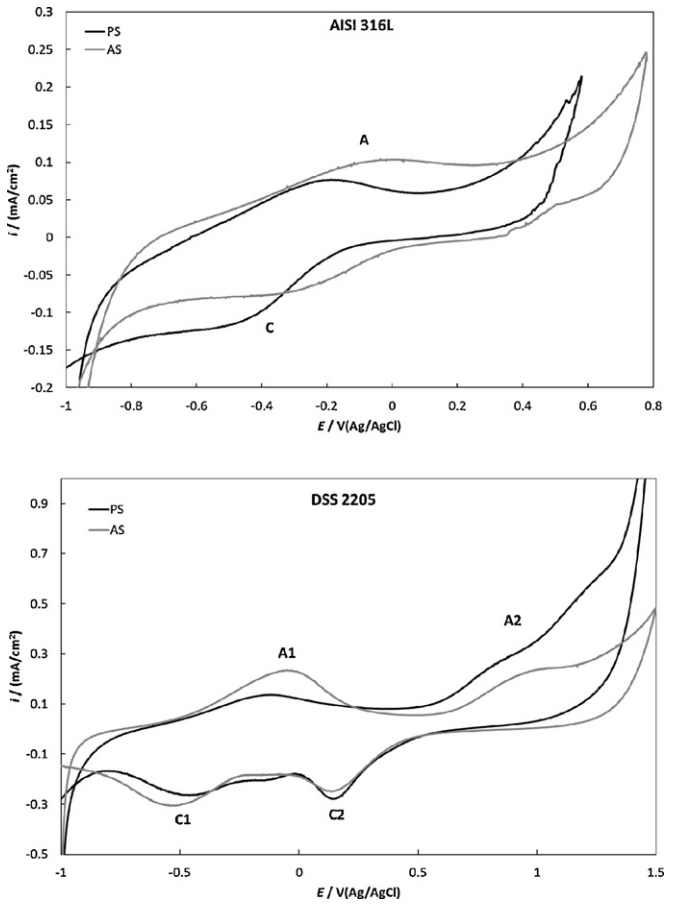

Fig. 1. Cyclic voltammograms recorded for AISI 316L and DSS 2205 stainless steels in AS and PS.

−1 V to 0.5 V and 1.5 V, respectively. As shown in Fig. 1, the main characteristics of the cyclic voltammograms of the two samples are similar in both solutions. In AS, four peaks are observed in the cyclic voltammogram for DSS 2205. The first anodic peak A1 at a potential of −0.2 V can be ascribed to electro-formation of Fe(II) hydroxide upon the Cr(III)-containing passivating layer, existing on the electrode at such potential values [18]. Another peak A2 is observed in the transpassive region, at 0.9 V, being associated with the oxidation of Cr(III) to Cr(VI) [19]. The Ni(II) species formed during the passivation process might have been oxidised to Ni(IV) oxide (NiO_2) in this potential range, too. In the reduction cycle at the potential of 0.2 V (peak C2), Cr(VI) was reduced to Cr(III) and the iron oxide-hydroxide layer was largely reduced in the potential range of the peak C1 at −0.5 V [19]. The measured breakdown potential for the DSS 2205 vs. Ag/AgCl in the AS was approximately 1.25 V [19].

When studying AISI 316L in AS, only two peaks were observed in the cyclic voltammograms. The first peak A at −0.2 V in the anodic cycle appears because of the electro-formation of Fe(II) hydroxide, while the second peak C at −0.5 V in the cathodic cycle corresponds to the reduction of iron oxide-hydroxide layer. The breakdown potential for the AISI 316L steel in AS is much lower, i.e., at 0.4 V [19].

In the PS solution, the cyclic voltammograms were similar to the results obtained for the AS. The main difference observed was the increase in the corrosion-current density due to increased chloride concentration in PS. In addition, the values of the breakdown potentials for the DSS 2205 and AISI 316L shifted to more negative potentials.

3.2. Atomic force microscopy

3.2.1. Surface morphology

The EC-AFM experiments generated topographic images showing the localized corrosion processes mainly associated with the increased concentration of chloride ions attacking the sample's structure.

Fig. 2a–d displays the surface of the DSS 2205 steel in both solutions, AS and PS, after exposure to specific potentiostatic conditions. AFM topography images indicate the samples' high pitting-corrosion resistance of the samples in both solutions, even when the samples were exposed to anodic potentials in the region of transpassive oxidation, i.e., 0.8 V and 1 V, for several minutes. The aggressive nature of PS due to increased chloride concentration, compared to AS, is however reflected in the reduced time scale of the DSS 2205 surface changes.

On the other hand, the surface of DSS 2205 in both solutions was marked by a protruding mass of square-like corrosion products, which grew as high regions on the AFM topography image (Fig. 2b and d). The deposition of the corrosion products observed in a surface oxide layer was a result of the formation of high state oxides, such as CrO_3, NiO_2 or Fe_3O_4 [19]. One can also see that the deposition process of oxide layers started uniformly (Fig. 2a and c), in continuous lines. With time and as the potentials were increased deeper into the region of transpassive oxidation, the deposition lines broke, resulting in several square-like protuberances covering the surface (Fig. 2b and d).

Fig. 3 compares the surface of the AISI 316L steel after an electrochemical treatment in each of the model solutions. The morphological structure of AISI 316L in AS is similar to the DSS 2205 sample, characterized by ellipse-like corrosion products growing extensively as the potential proceeded deeper into the region of transpassive oxidation, i.e., 0.5 V (Fig. 3b).

A different morphology was found when the AISI 316L steel was exposed to the PS solution (Fig. 3c and d). The sample was highly susceptible to corrosion and exhibited pronounced signs of attack by the enhanced concentration of Cl^- ions. Fig. 3c shows that many pits with different sizes and depths had formed already during the cyclic polarization test scan in the potential range −0.5 V to 0.8 V. The pitting was initiated by exposing the sample to slightly above the breakdown potential for only a few seconds, resulting in a current increase on the CV curve. The pits were accompanied by a protruding mass of corrosion products, shown as small bright spots on the AFM image. An additional exposure of the sample to an anodic potential of 0.5 V for 30 s, again lead to the extensive growth of ellipse-like corrosion deposits over the pits (Fig. 3d).

Some interesting features of the different corrosion products deposited on the surface of DSS 2205 and AISI 316L steels in both solutions were observed. The surface of DSS 2205 was covered with square-like deposits (Fig. 2b and d), whereas that of AISI 316L was characterized by ellipse-like deposits (Fig. 3b and d). The dissimilar morphology of the corrosion products is most probably related to the growth of oxides with different stoichiometries that dominate the surfaces the samples due to the altered chemical composition of the base materials, DSS 2205 and AISI 316L, as described in Section 2. It was reported by Brunet et al. [20], Estelle et al. [21] and Jasienska et al. [22] that chromium, nickel and iron oxides can crystallize in various morphologies depending on the oxygen content.

To obtain a further insight into the chemical composition of the oxide layers formed on the surface of both samples after oxidation in the transpassive region, the X-ray photoelectron spectroscopy (XPS) results are discussed in Section 3.2.3.

3.2.2. Surface roughness

The AFM topography images indicate that chloride ions eroded the surfaces of the specimens randomly. To determine the effect

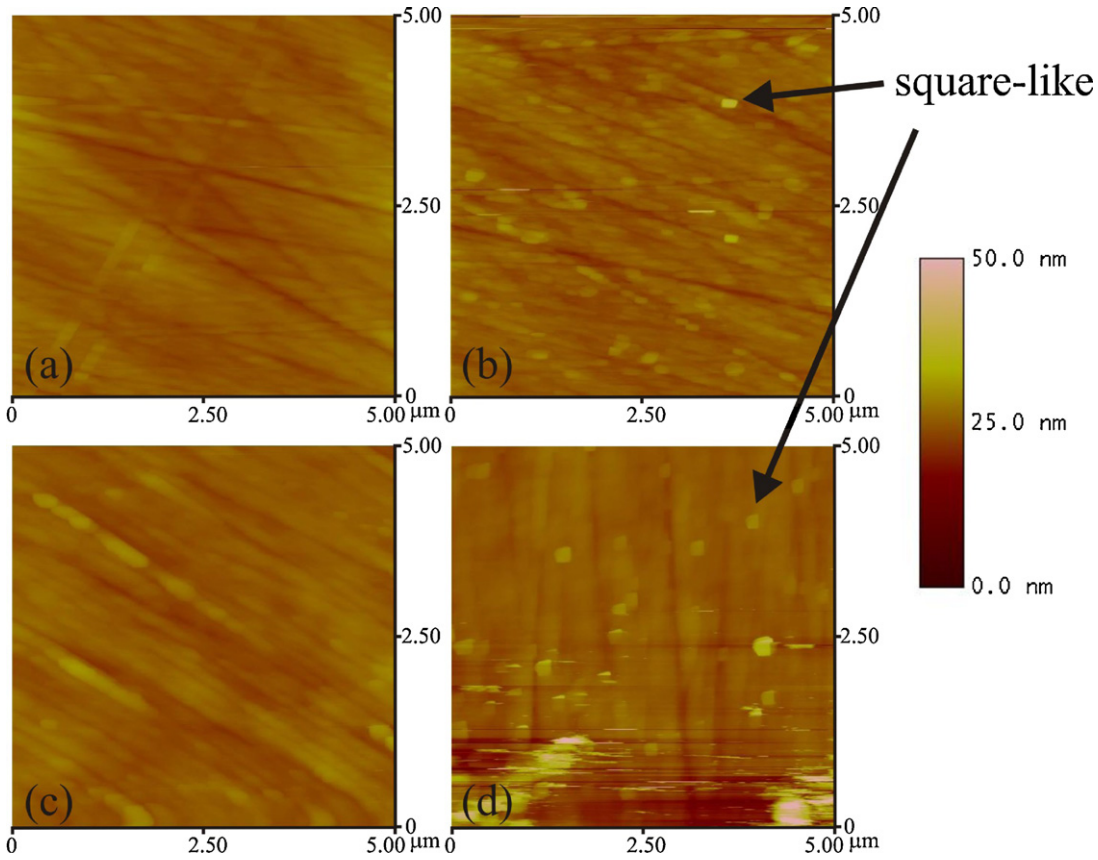

Fig. 2. AFM images of DSS 2205 sample: (a) in AS after being exposed to the potential of 0.8 V for 45 min, (b) in AS after additional exposure to the potential of 1 V for 11.6 min, (c) in PS after being exposed to the potential of 0.8 V for 17.2 min and (d) in PS after additional exposure to 1 V for 7.5 min. Here, one has to note, that the scanning angle was changed to 45° in order to exclude the possibility of the scanning artefact due to the homogeneity of the background sample. The scanned area was 5 μm × 5 μm; *z*-scales: 50 nm.

of the corrosion process on the surface roughness of the DSS 2205 and AISI 316L in AS and PS solutions, surface profile measurements received additional attention in EC-AFM measurements. The Veeco NanoScope software 5.12r5 offers the possibility to calculate the average surface roughness, Ra, for each sample from the AFM surface topographic data in a scanning area of 5 μm × 5 μm (as set by the operator) using the equation:

$$\mathrm{Ra} = \frac{1}{MN}\sum_{i=1}^{M}\sum_{j=1}^{N}|Z(x_i, y_j)| \quad (1)$$

where $Z(x_i, y_j)$ denotes the height of a surface point (x_i, y_j) relative to the mean plane and MN is the number of points in the analyzed area.

Fig. 4 shows the variation of the average surface roughness (Ra) values of DSS 2205 and AISI 316L surfaces under various potentiostatic conditions (i.e., the time of exposure to different anodic potentials, as described in Figs. 2 and 3) in AS and PS solutions. It can be seen that the values of the parameter Ra are directly related to the corrosivity of the surface. As described in Section 3.2.2, the highly resistant DSS 2205 surface hardly responded to potentiostatic treatment in both solutions. The slight increase in the average surface-roughness values is therefore mainly connected to the growth of the corrosion products. The average surface roughness is, therefore, in the nanometre range, indicating the nanoscale growth of corrosion products extending up to a few tenths of nanometres in the z-direction and up to 200 nm in the lateral directions. A similar dependence was observed for the AISI 316L surface in AS solution. However, there is a large increase in Ra of AISI 316L in PS solution due to the increased concentration of chloride ions in the PS compared to the AS solution.

Table 1
The composition of the oxide layer formed on 2205 DSS in AS.

E/V	% Cr	% Cr-ox	% Fe	% Fe-ox	% Mo	% Mo-ox	% Ni	% Ni-ox	% Mn
0	9.84	57.37	8.46	13.93	1.54	1.77	3.89	0.63	2.56
1.5	2.00	39.08	3.25	55.35	0.03	0.20	0.06	0.03	0.00

3.2.3. X-ray photoelectron spectroscopy

The XPS measurements gave us an insight into the average chemical composition of the oxide layers formed at the surface of both samples after the exposure to the selected potentials, i.e., in the region of passive behaviour and in the region of transpassive oxidation. For this purpose, the XPS spectra were recorded after exposure at potentials of special interest, in close correlation to the cyclic voltammograms. The samples were oxidised at the selected potentials for 30 min prior to the XPS measurements.

Tables 1–4 present the composition of the oxide layer after the oxidation of DSS 2205 and AISI 316L steels in AS and PS solutions. In both solutions the fraction of Fe at the oxide layer of both

Table 2
The composition of the oxide layer formed on 2205 DSS in PS.

E/V	% Cr	% Cr-ox	% Fe	% Fe-ox	% Mo	% Mo-ox	% Ni	% Ni-ox	% Mn
0	10.79	70.03	9.29	5.51	1.68	1.03	1.08	0.59	0.00
1.5	4.14	39.52	0.66	53.02	0.02	0.19	1.37	1.083	0.00

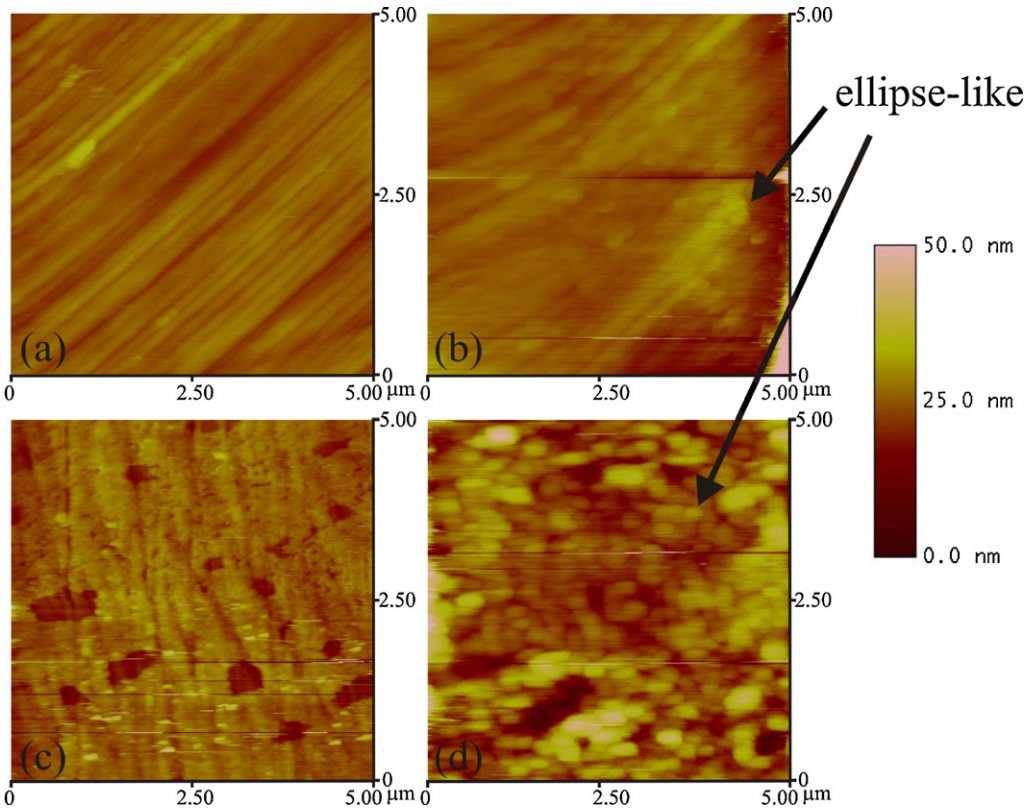

Fig. 3. AFM image of AISI 316L sample: (a) in AS after exposing the sample to anodic potential of 0.5 V for 10 min, (b) in AS after additional exposure of the sample to 0.5 V for 6.6 min, (c) in PS immediately after the test cyclic voltammogram in the range of potentials from −0.5 V to 0.8 V and (d) in PS after additional exposure to 0.5 V for 30 s. The scanned area was 5 μm × 5 μm; *z*-scales: 50 nm.

Table 3
The composition of the oxide layer formed on AISI 316L in AS.

E/V	% Cr	% Cr-ox	% Fe	% Fe-ox	% Mo	% Mo-ox	% Ni	% Ni-ox	% Mn
0	9.32	52.88	7.16	20.11	1.37	2.56	4.49	0.02	2.09
0.65	3.76	15.44	1.85	64.88	0.63	9.30	1.11	0.67	2.35

investigated materials was less than that of the bulk concentration, and this effect increased with the increased chloride concentration. The passive layer was Cr-enriched compared to the bulk concentration; the Cr concentration was higher at lower potentials and decreased at higher anodic potentials. The concentration of Ni was strongly reduced compared to the bulk concentration; that of the Mo increased at higher anodic potentials compared to the bulk concentration.

The main constituent of the oxide layer formed at the surface of DSS 2205 after oxidation at 0 V in both solutions was Cr-oxide and the total amount of Cr was enriched compared to the bulk concentration. The second major constituent of the passive layer was Fe-oxide, although the total amount of Fe was lower than in the bulk. The amounts of Mo- and Ni-oxides were very low, especially for Ni, in comparison to the bulk. With increasing chloride concentration in the PS solution, the amounts of Fe and Ni species decreased due to preferential dissolution in the presence of chloride ions. Clayton and Lu [23] emphasized that Ni was rarely observed in the passive films of stainless steels formed in solutions containing chloride ions. Therefore, the amount of Cr-oxide increased.

After oxidation at 1.5 V, the oxide layer predominantly consisted of Fe-oxides and was slightly depleted in Cr-oxide compared to the results at 0 V, due to effects explained later. From the equilibrium diagrams of chromium it is expected that at potentials anodic to 0 V, chromium would dissolve preferentially [18]. The XPS results confirmed this prediction: when DSS was passivated at potentials ≥0 V, the chromium level slightly decreased and that of the iron increased towards the oxide-solution interface. The amounts of Ni and Mo species were significantly depleted.

Table 4
The composition of the oxide layer formed on AISI 316L in PS.

E/V	% Cr	% Cr-ox	% Fe	% Fe-ox	% Mo	% Mo-ox	% Ni	% Ni-ox	% Mn
0	9.71	62.87	8.35	16.86	0.38	1.32	0.14	0.37	0.00
0.65	0.01	21.87	0.00	60.80	1.76	13.75	0.29	1.52	0.00

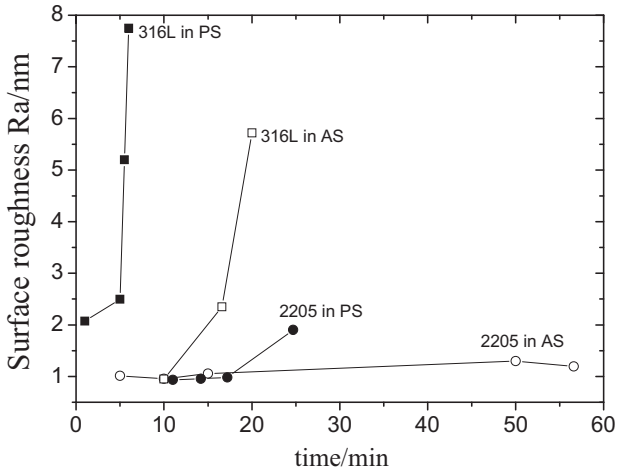

Fig. 4. The variation of average surface roughness (Ra) of DSS 2205 in AS (○) and PS (●) and of AISI 316L in AS (□) and PS (■) with time under various potentiostatic conditions as described in Figs. 2 and 3.

Similar results were obtained for AISI 316L, however, with a slightly higher content of Fe in the oxide layer compared to the DSS 2205.

4. Conclusions

A combined electrochemistry atomic force microscopy study was implemented to investigate the effect of localized corrosion and the morphology changes of duplex stainless steel of the type 2205 (DSS 2205) and austenitic stainless steel AISI 316L when electrochemically treated in artificial saliva (AS) and a simulated physiological solution, i.e., – Hank's solution (PS), which was characterized by a higher chloride concentration thank the AS.

AFM topography studies illustrated the high corrosion resistance of DSS 2205 in both solutions for the chosen range of electrochemical potentials applied to the sample. The AISI 316L steel was stable against corrosion in AS; however, it was highly susceptible to pitting in PS due to the increased chloride content. The morphology of both surfaces was enriched with the growth of corrosion products during the oxidation process in the surface oxide layer. We distinguished between the square-like and ellipse-like deposits on the surface of DSS 2205 and AISI 316L, respectively; the dissimilar shapes being related to the growth of Cr, Fe and Ni oxides with different stoichiometries that dominated the samples' surfaces due to the altered chemical composition of the base materials.

In both investigated materials, the average surface roughness (Ra) values in the nanometre range were mainly a result of the growth of corrosion products and reflected the degree of the samples' corrosivity and the nanometre dimensions of the deposits.

The XPS results obtained in the present work revealed that the oxide film formed on the surface of DSS 2205 and AISI 316L steels in both investigated solutions contained oxides of two main elements, i.e., Fe and Cr. The oxides of the alloying elements Ni and Mo were negligible compared to the bulk, except for the increased Mo concentration in the transpassive region.

Generally speaking, DSS 2205 is considered to be a promising material for medical applications due to the increased corrosion resistance compared to AISI 316L stainless steel, as confirmed by the present study. The main improvement with respect to medical applications is the decrease in the nickel hypersensitivity effect for patients undergoing medical treatments, with the advantage of the reduced nickel content in DSS 2205. This demonstrates the suitability of 2205 DSS for medical applications in artificial saliva and simulated physiological solutions.

Acknowledgements

This work was carried out within the framework of the Slovene programme P2-0132, "Fizika in kemija površin kovinskih materialov" of Slovenian Research Agency, whose support is gratefully acknowledged by M. Conradi and A. Kocijan. P.M. Schön and G.J. Vancso acknowledge the Netherlands Foundation for Scientific research (NWO) and the University of Twente for funding.

References

[1] T. Hryniewicz, R. Rokicki, K. Rokosz, Corrosion 64 (2008) 660–665.
[2] M. Finsgar, S. Fassbender, S. Hirth, I. Milosev, Mater. Chem. Phys. 116 (2009) 198–206.
[3] R.M. Souto, I.C.M. Rosca, S. Gonzalez, Corrosion 57 (2001) 300–306.
[4] J. Pan, C. Karlen, C. Ulfvin, J. Electrochem. Soc. 147 (2000) 1021–1025.
[5] M. Dabala, I. Calliari, A. Variola, J. Mater. Eng. Perform. 13 (2004) 237–240.
[6] F. Bernard, V.S. Rao, H.S. Kwon, J. Electrochem. Soc. 152 (2005) B415–B420.
[7] P.J. Antony, S. Chongdar, P. Kumar, R. Raman, Electrochim. Acta 52 (2007) 3985–3994.
[8] A. Kocijan, C. Donik, M. Jenko, Mater. Technol. 43 (2009) 39–42.
[9] A. Kocijan, C. Donik, M. Jenko, Mater. Technol. 43 (2009) 195–199.
[10] E.C. Souza, S.M. Rossitti, J. Rollo, Mater. Charact. 61 (2010) 240–244.
[11] A. Kocijan, I. Milosev, B. Pihlar, J. Mater. Sci. Mater. Med. 14 (2003) 69–77.
[12] G.T. Burstein, C. Liu, Corros. Sci. 49 (2007) 4296–4306.
[13] A. Shahryari, S. Omanovic, J.A. Szpunar, J. Biomed. Mater. Res. A 89A (2009) 1049–1062.
[14] F.J. Torres, W. Panyayong, W. Rogers, D. Velasquez-Plata, Y. Oshida, B.K. Moore, Biomed. Mater. Eng. 8 (1998) 2–36.
[15] L. Veleva, M.A. Alpuche-Aviles, M.K. Graves-Brook, D.O. Wipf, J. Electroanal. Chem. 537 (2002) 85–93.
[16] D.A. Shirley, Phys. Rev. B 5 (1972) 4709–4714.
[17] N. Fairley, CasaXPS VAMAS Processing Software , 1999 , http://www.casaxps.com/.
[18] N. Ramasubramanian, N. Preocanin, R.D. Davidson, J. Electrochem. Soc. 132 (1985) 793–798.
[19] A. Kocijan, D. Kek Merl, M. Jenko, Corros. Sci. 53 (2) (2011) 776–783.
[20] S. Brunet, B. Boussand, A. Rousset, Appl. Catal. A: Gen. 168 (1998) 57–61.
[21] J. Estelle, P. Salagre, Y. Cesteros, M. Serra, F. Medina, J.E. Sueiras, Solid State Ionics 156 (2003) 233–243.
[22] S. Jasienska, J. Janowski, M. Ghodsi, G. Naessens, Solid State Ionics 12 (1984) 449–452.
[23] C.R. Clayton, Y.C. Lu, J. Electrochem. Soc. 133 (1986) 2465–2473.